Available online at www.sciencedirect.com
ScienceDirect
Composites Science and Technology 66 (2006) 2997–3003
COMPOSITES SCIENCE AND TECHNOLOGY
www.elsevier.com/locate/compscitech

Material modeling of the CVI-infiltrated carbon felt I: Basic formulae, theory and numerical experiments

R. Piat [a,*], I. Tsukrov [b], N. Mladenov [a], V. Verijenko [c], M. Guellali [d], E. Schnack [a], M.J. Hoffmann [d]

[a] Institute of Solid Mechanics, University of Karlsruhe, Kaiserstr.12, D-76128 Karlsruhe, Germany
[b] Department of Mechanical Engineering, University of New Hampshire, Durham, NH 03824, USA
[c] School of Mechanical Engineering, University of Kwazulu-Natal, Durban 4041, South Africa
[d] Institute of Ceramics in Mechanical Engineering, Central Laboratory, University of Karlsruhe, Haid-und-Neu-Str. 7, D-76131 Karlsruhe, Germany

Received 15 September 2005; received in revised form 26 January 2006; accepted 5 February 2006
Available online 29 March 2006

Abstract

A material model for predicting the unknown elastic properties of the chemical vapor infiltrated carbon felts is proposed. Representative volume element of the studied material includes pyrolytic carbon matrix, randomly distributed carbon fibers (carbon felt) and pores. The homogenization procedure for this composite consists of two steps: (1) homogenization of material response without pores, i.e., homogenization of a media consisting of carbon fibers randomly distributed in an isotropic pyrolytic carbon matrix; (2) homogenization of material response with presence of pores, i.e., homogenization of a media consisting of three-dimensional pores embedded in the homogenized matrix from the previous step. The proposed model constitutes a theoretical basis for the numerical analysis of various carbon/carbon material systems that will be presented in the consecutive publications.

Keywords: A. Carbon–carbon composites; B. Modelling; B. Microstructure; C. Elastic properties; E. Chemical vapour infiltration (CVI)

1. Introduction

Isothermal, isobaric chemical vapor infiltration (I-CVI) is widely used to produce carbon/carbon (C/C) composites for high tech applications such as in aeronautical and space industries [1]. Understanding of the relationship between the complex microstructure of these materials (distribution of the carbon fibers and that of the pores, texture of the deposited pyrocarbon matrix [2]) and their mechanical properties is essential in order to assess their full performance potential for more advanced service applications. However, micromechanical modelling of I-CVI densified carbon/carbon composites presents several challenges. Firstly, the constituents in the composite have different length scales: the diameter of fibers used in such composites is on the order of 10 μm while some pores reach up to hundreds of microns in dimensions. Secondly, pores are of irregular shapes, and cannot be easily analysed using available elasticity solutions. And finally, the distribution of pores and the texture and, consequently, the mechanical properties of the pyrolytic carbon matrix are highly dependent on the manufacturing parameters (pressure and temperature distribution during infiltration).

To overcome these difficulties, this paper proposes a homogenization procedure which consists of two steps: (1) homogenization of material response without pores, i.e., homogenization of a media consisting of carbon fibers randomly distributed in an isotropic pyrolytic carbon matrix; (2) homogenization of material response with presence of pores, i.e., homogenization of a media consisting of three-dimensional pores embedded in the homogenized matrix from the previous step.

The paper is organized as follows. Section 2 gives more details on the CVI technology and provides typical examples of the microstructure of carbon fiber felt composites

* Corresponding author. Tel.: +49 7216088853; fax: +49 7216084187.
E-mail address: Romana.Piat@mach.uni-karlsruhe.de (R. Piat).

0266-3538/$ - see front matter © 2006 Elsevier Ltd. All rights reserved.
doi:10.1016/j.compscitech.2006.02.008

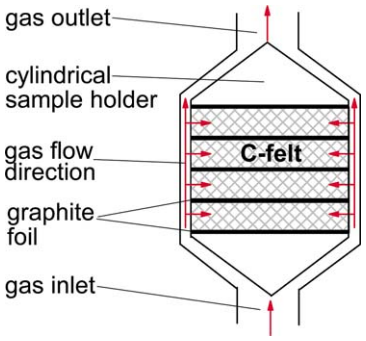

Fig. 1. Experimental setup.

(CFCs). Section 3 presents the theory of micromechanical modeling of these composites indicating all the assumptions and approximations made to obtain the closed form predictions of the effective elastic properties. The numerical simulation results for two types of CFCs are presented in Section 4. Several possible pore distributions are computer generated using a random number generator, and the influence of pore shapes on the overall properties is discussed.

2. Typical microstructures of I-CVI densified C/C composites

The investigated samples are carbon fiber felts (CCKF 1001, Sintec, Germany) with initial relative porosity of 88 vol.% infiltrated by means of the I-CVI process at a temperature of 1100 °C. The infiltration was carried out by the group of Prof. Hüttinger at the Institute for Chemical Technology of the University of Karlsruhe, Germany. Fig. 1 shows the experimental setup used. Further details on the infiltration procedure are given elsewhere [3,4].

The PAN-fibers forming the felts have a typical diameter of 12 μm and are randomly oriented (Fig. 2a). The felt infiltrated at 1095 °C, using pure methane at a total pressure of 10 kPa during 150 h is presented on Fig. 2b and felt infiltrated at 1070 °C, at 30 kPa methane pressure during 120 h is presented on Fig. 2c.

3. Material modelling

To predict the effective elastic properties of CVI CFCs we generalize the two-step homogenization procedure initially proposed in [5] for unidirectional carbon/carbon composites. We first homogenize the material consisting of pyrolytic carbon matrix with randomly distributed carbon fibers, and then account for contribution of pores as described below.

3.1. Non-interaction and Mori–Tanaka homogenization procedures for pyrolytic carbon matrix with randomly distributed fibers

Firstly, we homogenize material consisting of pyrolytic carbon matrix and randomly distributed carbon fibers. For this homogenizations step, carbon fibers are approximated by randomly oriented needle-shaped inclusions. Several micromechanical schemes have been proposed in literature to model such materials, see, for example, [6]. They differ, mostly, by how interaction between individual fibers is taken into account. However, as shown in [7], predictions of several most popular schemes can be readily obtained if the non-interaction approximation of the effective elastic properties is known. In this paper, we provide the non-interaction and Mori–Tanaka predictions of the overall material properties. The non-interaction approximation of the compliance tensor of the material is given by [7]:

$$D^{\mathrm{MF}}_{ijkl} = D^{M}_{ijkl} + \frac{f_I}{100}\left[h_1\delta_{ij}\delta_{kl} + h_2\left(\delta_{ik}\delta_{jl} + \delta_{il}\delta_{jk} - \frac{2}{3}\delta_{ij}\delta_{kl}\right)\right], \tag{1}$$

where

$$h_1 = \frac{(k_M - k_I)[\mu_M(4k_I - k_M) + k_M(3k_I + \mu_I)]}{9k_I k_M^2(3k_I + \mu_I + 3\mu_M)} \text{ and}$$

$$h_2 = \frac{\mu_M - \mu_I}{5\mu_M}\left[\frac{2}{\mu_M + \mu_I} + \frac{6k_M + 8\mu_M}{3k_M\mu_I + 7\mu_I\mu_M + 3k_M\mu_M + \mu_M^2} - \frac{4\mu_I + k_I}{4\mu_I^2} + \frac{(3k_I + 4\mu_I)(k_I + \mu_I)}{4\mu_I^2(3k_i + \mu_I + 3\mu_M)}\right]$$

If the Mori–Tanaka micromechanical scheme for interacting fibers is used [8,9], then

$$D^{\mathrm{MF}}_{ijkl} = D^{M}_{ijkl} + \frac{f_I}{100}\left[h_3\delta_{ij}\delta_{kl} + h_4\left(\delta_{ik}\delta_{jl} + \delta_{il}\delta_{jk} - \frac{2}{3}\delta_{ij}\delta_{kl}\right)\right], \tag{2}$$

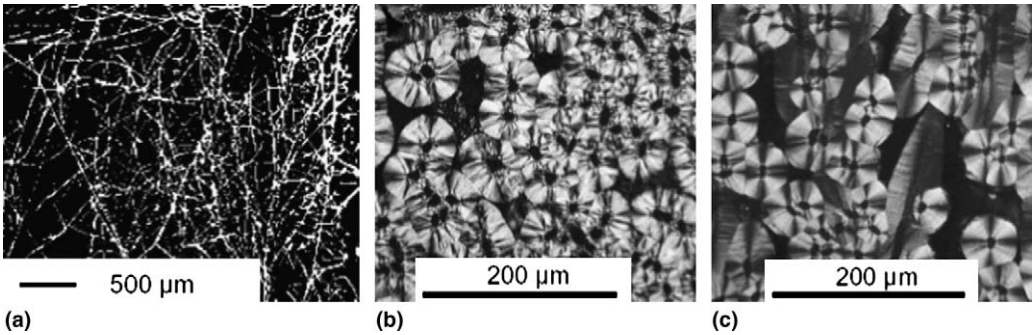

Fig. 2. (a) SEM micrograph of the carbon fiber felt as received (b) and (c) PLM micrographs of the investigated samples.

where

$$h_3 = \frac{(k_M - k_I)[\mu_M(4k_I - k_M) + k_M(3k_I + \mu_I)]}{9k_I k_M^2(3k_i + \mu_I + 3\mu_M) - 0.36 f_I k_I k_M \mu_M (k_M - k_I)} \text{ and}$$

$$h_4 = h_3\left(1 - h_3 \frac{f_I}{100}\frac{4\mu_M\mu_I}{\mu_M - \mu_I}\right)^{-1}.$$

In these formulas, D^M_{ijkl} is the compliance tensor of the matrix material, δ_{ij} is the Kronecker's delta, f_I is the volume fraction of fibers, k_I and k_M are the bulk moduli, and μ_I and μ_M are the shear moduli of fibers and matrix. These moduli can be expressed in terms of the Young's modulus E and Poisson's ratio v as

$$\mu = \frac{E}{2(1+v)}, \quad k = \frac{E}{3(1-2v)}.$$

3.2. Homogenization procedure for the effective matrix consisting of fibers and pyrolytic carbon with pores

3.2.1. Eshelby solution for prolate and oblate spheroids

Next step of the homogenizations procedure is to insert the pores in the homogenized material of the last step consisting of pyrolytic carbon matrix and fibers. The pores are three-dimensional and their shapes are irregular, so the problem is very complicated. In the homogenization, we will approximate the irregular shapes of the pores as spheroids with semi-axes a_1, a_2 and a_3 such that

$$a_1 = a_2 \text{ and } a_3/a_1 = \alpha. \tag{3}$$

For $\alpha < 1$ we obtain prolate and for $\alpha > 1$ oblate spheroids (see Fig. 3a and b).

Elastic fields around ellipsoidal inclusions are expressed in terms of the so-called Eshelby tensor **S** [10]. To find the components of this tensor for spheroidal pores we must calculate parameter g [11], which is different for prolate and oblate spheroids. For prolate spheroids,

$$g = \frac{\alpha}{(\alpha^2-1)^{3/2}}\left[\alpha(\alpha^2-1)^{1/2} - \operatorname{arccosh}\alpha\right], \quad \alpha > 1 \tag{4}$$

and for oblate spheroids,

$$g = \frac{\alpha}{(1-\alpha^2)^{3/2}}\left[\arccos\alpha - \alpha(1-\alpha^2)^{1/2}\right], \quad \alpha < 1. \tag{5}$$

Then the components of the Eshelby tensor are

$$\begin{aligned}
S_{1111} &= S_{2222} = -\frac{3\alpha^2}{8(1-v)(1-\alpha^2)} + \frac{g}{4(1-v)}\left[1-2v+\frac{9}{4(1-\alpha^2)}\right],\\
S_{3333} &= \frac{1}{1-v}\left[2-v-\frac{1}{1-\alpha^2}\right] + \frac{g}{2(1-v)}\left[-4+2v+\frac{3}{1-\alpha^2}\right],\\
S_{1122} &= S_{2211} = \frac{1}{8(1-v)}\left[1-\frac{1}{1-\alpha^2}\right] + \frac{g}{16(1-v)} \times \left[-4(1-2v)+\frac{3}{1-\alpha^2}\right],\\
S_{1133} &= S_{2233} = \frac{\alpha^2}{2(1-v)(1-\alpha^2)} - \frac{g}{4(1-v)}\left[1-2v+\frac{3\alpha^2}{1-\alpha^2}\right],\\
S_{3311} &= S_{3322} = \frac{1}{2(1-v)}\left[-(1-2v)+\frac{1}{1-\alpha^2}\right] + \frac{g}{4(1-v)} \times \left[2(1-2v)-\frac{3}{1-\alpha^2}\right],\\
S_{1212} &= -\frac{\alpha^2}{8(1-v)(1-\alpha^2)} + \frac{g}{16(1-v)}\left[4(1-2v)+\frac{3}{1-\alpha^2}\right],\\
S_{1313} &= S_{2323} = \frac{1}{4(1-v)}\left[1-2v+\frac{1+\alpha^2}{1-\alpha^2}\right] - \frac{g}{8(1-v)} \times \left[1-2v+3\frac{1+\alpha^2}{1-\alpha^2}\right],
\end{aligned} \tag{6}$$

where v is the Poisson's ratio of the homogenized matrix. The remaining components of this tensor can be calculated from symmetry properties:

$$S_{ijkl} = S_{jikl} = S_{ijlk} = S_{jilk}.$$

3.2.2. Compliance tensor of an ellipsoidal pore

To calculate the compliance contribution tensor **H** for each pore of volume $V^* = 4\pi a_1 a_2 a_3/3$ in the RVE of volume V we can use the following formulae [11]:

$$\begin{aligned}
H_{1111} &= \frac{V^*}{V E \Delta}\{(1-S_{2222})(1-S_{3333}) - S_{2233}S_{3322} - v[S_{1122}(1-S_{3333}+S_{2233}) + S_{1133}(1-S_{2222}+S_{3322})]\}\\
H_{1122} &= \frac{V^*}{V E \Delta}\{S_{1122}(1-S_{3333}) + S_{1133}S_{3322} - v[(1-S_{2222}) \times (1-S_{3333}+S_{1133}) + S_{2233}(S_{1122}-S_{3322})]\},
\end{aligned}$$

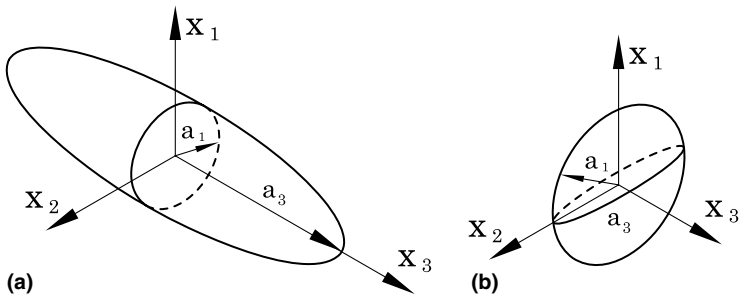

Fig. 3. (a) Prolate spheroid. (b) Oblate spheroid.

$$H_{1212} = \frac{V^*}{VE}\frac{1+v}{2(1-2S_{1212})} \tag{7}$$

In the formulae above

$$\Delta = -\det\begin{bmatrix} S_{1111}-1 & S_{1122} & S_{1133} \\ S_{2211} & S_{2222}-1 & S_{2233} \\ S_{3311} & S_{3322} & S_{3333}-1 \end{bmatrix},$$

S_{ijkl} are the components of the Eshelby tensor for each ellipsoid, and E and v are the Young's modulus and Poisson's ratio of the material consisting of carbon fibers randomly distributed in the pyrolytic carbon matrix. These parameters can be calculated using the components of the compliance tensor obtained in the previous step of the homogenization procedure:

$$E = \frac{1}{D^{\mathrm{MF}}_{1111}}; \quad v = -\frac{D^{\mathrm{MF}}_{1122}}{D^{\mathrm{MF}}_{2222}}.$$

The remaining terms of tensor **H** can be calculated from symmetry properties.

3.2.3. Compliance contribution tensor of all pores in the global coordinate system

The obtained components of the compliance contribution tensor **H** of each pore are given in the local coordinate system of the pore. To evaluate contributions of all pores to the effective elastic properties of the material, we have to perform transformation from local to the global coordinate system common to all pores. Fig. 4 presents relative orientation of these two coordinate systems. Axes 1, 2 and 3 define the local orthogonal coordinate system of the pore used in formulae (7). The components of the compliance tensor $\mathbf{H}^{\mathrm{tr}}$ (presented in the matrix form) in global coordinate system X_1, X_2, X_3 and local coordinate system 1, 2, 3 are related as

$$[\mathbf{H}^{\mathrm{tr}}] = [\mathbf{L}]^{\mathrm{T}}[\mathbf{L}]^{\mathrm{T}}[\mathbf{H}][\mathbf{L}][\mathbf{L}]. \tag{8}$$

where [**L**] is the transformation matrix given by [8]:

$$[\mathbf{L}] = \begin{pmatrix} \cos\theta\cos\beta\cos\phi - \sin\beta\sin\phi & -\cos\theta\cos\beta\sin\phi - \sin\beta\cos\phi & \sin\theta\cos\beta \\ \cos\theta\sin\beta\cos\phi + \cos\beta\sin\phi & -\cos\theta\sin\beta\sin\phi + \cos\beta\cos\phi & \sin\theta\sin\beta \\ -\sin\theta\cos\phi & \sin\theta\sin\phi & \cos\theta \end{pmatrix}. \tag{9}$$

After application of this procedure to all pores, using the non-interaction model, the overall compliance contribution tensor of the pores $\mathbf{H}^P$ can be calculated as:

$$\mathbf{H}^P = \sum_i \mathbf{H}^{\mathrm{tr}}_i. \tag{10}$$

Then the effective compliance of the material with pores $\mathbf{D}^{\mathrm{eff}}$ is

$$\mathbf{D}^{\mathrm{eff}} = \mathbf{D}^{\mathrm{NI}} + \mathbf{H}^P \text{ or } \mathbf{D}^{\mathrm{eff}} = \mathbf{D}^{\mathrm{MT}} + \mathbf{H}^P. \tag{11}$$

4. Numerical results

4.1. Evaluation of the effective elastic properties of the material consisting of fibers in the pyrolytic carbon matrix

On the nanoscale, pyrolytic carbon is an anisotropic material with mechanical properties depending on the orientation with respect to the nearest fiber surface. Its stiffness is determined by the pressure and temperature distribution during infiltration. But on the microscale, for randomly oriented structures, the overall response of pyrolytic carbon can be assumed to be isotropic.

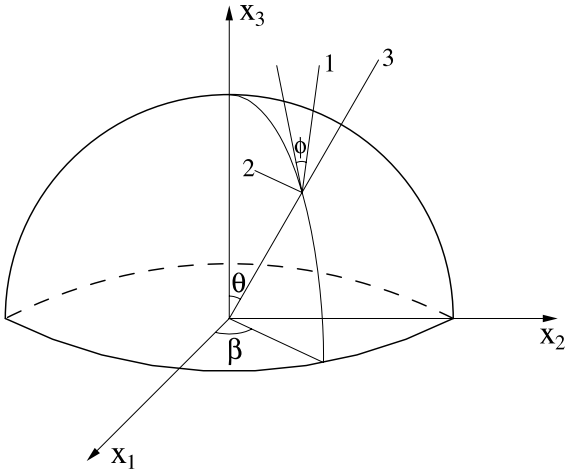

Fig. 4. A random orientation of an ellipsoidal pore is described by a point of the unit sphere. The local coordinates of the pore are given by the axes 1,2,3 [8].

Table 1 provides the material properties of the carbon felt and two sets of material constants for pyrolytic carbon (PyC 1 and PyC 2) that we used in our simulations. The corresponding homogenized materials are denoted as M1 and M2. Using these parameters and Eqs. (1) and (2), we obtain the non-interaction and Mori–Tanaka predictions of the homogenized material properties (Young's modulus and Poisson's ratio) for various volume fractions of fibers. The results for Young's modulus and Poisson's ratio are presented in Figs. 5 and 6 correspondingly. The Poisson's ratio values for two materials are practically identical, and that's why only one graph is presented.

To analyze the difference between the non-interaction and Mori–Tanaka approximations, we utilized the following formulae:

$$Dif_E = \frac{|E^{\mathrm{MT}} - E^{\mathrm{NI}}|}{E^{\mathrm{MT}}} \cdot 100\%;$$

$$Dif_v = \frac{|v^{\mathrm{MT}} - v^{\mathrm{NI}}|}{v^{\mathrm{MT}}} \cdot 100\% \tag{12}$$

Table 1
Elastic properties of isotropic pyrolytic carbon and carbon felt [12,13]

Pyrolytic carbon				Carbon felt	
PyC 1		PyC 2			
E_{m1} (GPa)	v_{m1}	E_{m2} (GPa)	v_{m2}	E_f (GPa)	v_f
25.0	0.15785	38.556	0.16	200	0.27

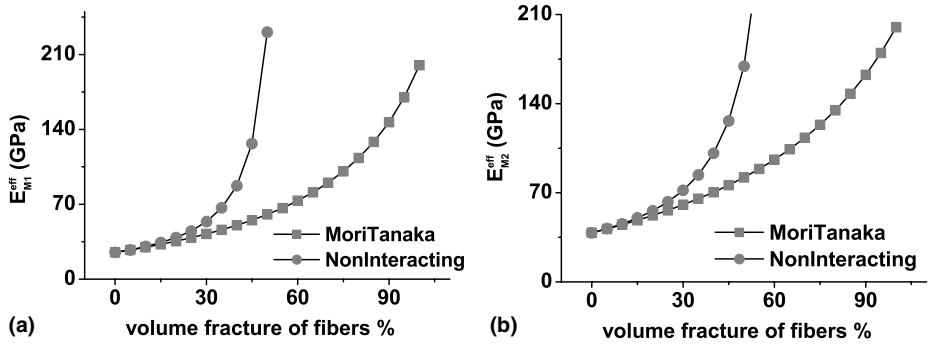

Fig. 5. Effective Young's moduli $E^{\text{eff}}_{\text{M1}}$ and $E^{\text{eff}}_{\text{M2}}$ for homogenized material consisting of carbon fibers randomly distributed in the pyrolytic carbon matrix: (a) PyC 1 and (b) PyC 2.

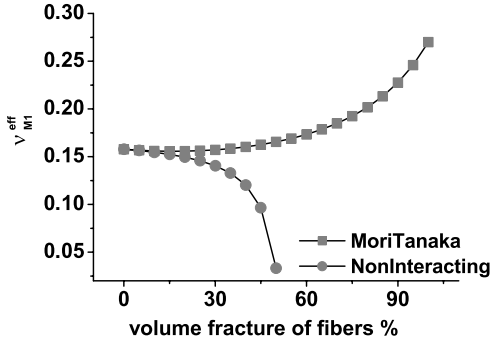

Fig. 6. Effective Poisson's ratio $\nu^{\text{eff}}_{\text{M1}}$ for homogenized material consisting of carbon fibers randomly distributed in the pyrolytic carbon matrix PyC 1.

Table 2
Material parameters of the homogenized material, which consists of PyC-matrix with 12% volume fraction of fibers

M	Non-interacting		Mori–Tanaka	
	E^{NI} (GPa)	ν^{NI}	E^{MT} (GPa)	ν^{MT}
M1	31.81	0.15375	30.87	0.15582
M2	47.33	0.15868	46.29	0.15951

Table 3
Number of oblate and prolate spheroids generated for different porosities using random number generator

Porosity	Number of prolate spheroids	Number of oblate spheroids
0.02	97	113
0.04	218	232
0.06	311	338
0.08	405	522
0.10	449	613
0.12	636	713
0.14	645	819
0.16	768	997
0.18	912	1012
0.20	1010	1122

For different volume fractions of the fibers this difference is presented in Fig. 7.

Analysis of the results shows that for small volume fractions of fibers both approximations produce very close predictions of the effective Young's moduli and Poisson's ratio. For example, at 15% and 20% of fiber volume fraction, the deviation in the Young's moduli is 3.7% for M1 (0.5% for M2) and 7% for M1 (0.93% for M2), correspondingly. For the Poisson's ratio this difference is even smaller.

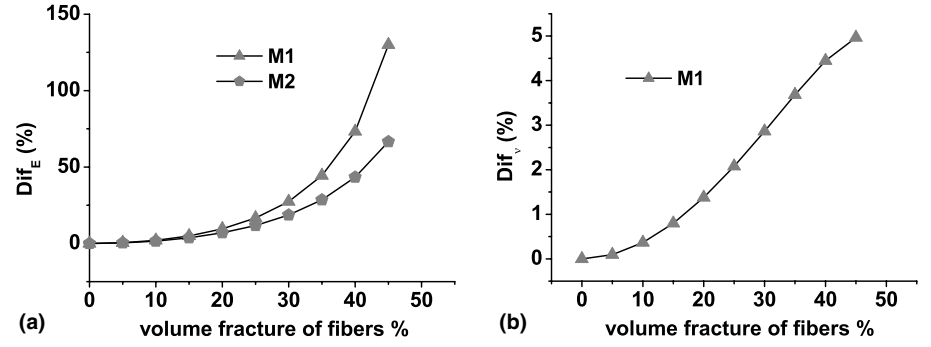

Fig. 7. Difference between the non-interaction and Mori–Tanaka approximations of: (a) effective Young's moduli for M1 and M2; (b) effective Poisson's ratio for M1 as function of the fiber volume fraction.

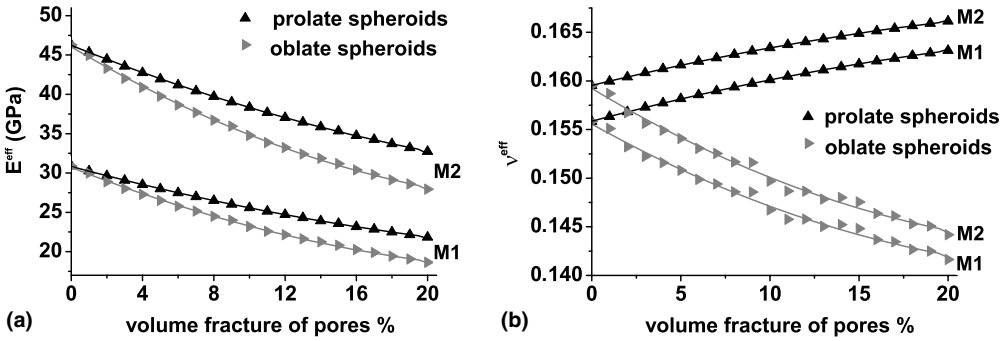

Fig. 8. Values of the effective Young's moduli and Poisson's ratios calculated for pore models as prolate and oblate spheroids.

Thus, the obtained predictions for the composites described in Section 2 having 12% of fiber volume fraction are practically identical for both methods (Table 2).

4.2. Evaluation of the effective elastic properties of the composite

In the infiltrated felts, random orientation of fibers leads to random orientations and shape distributions of pores in the produced composite. That's why for numerical modeling of this material we can use a random number generator to generate ellipsoidal pores with random orientational distribution and different volume fractions. The simulations were performed for two distinct cases: for all prolate and for all oblate spheroids. The limits for the spheroid eccentricity parameter α (see (3)) were chosen based on the micrographical observations of actual materials: $0.14 < \alpha < 0.67$ for prolate and $1.5 < \alpha < 07$ for oblate spheroids. The examples of generated microstructures are presented in Table 3. For randomly generated pores from the Table 3, the compliance tensors and then the effective Young's moduli and Poisson's ratios as functions of porosity were calculated. The results for oblate and prolate models of pores for materials M1 and M2 are presented in Fig. 8. Note that the pore configuration in the real material is such that both approximations, oblate and prolate spheroids, have to be used. Thus, the obtained curves for effective Young's moduli and Poisson's ratios can be considered as the upper (only prolate spheroids) and lower (only oblate spheroids) bounds for real material.

5. Conclusions

The proposed micromechanical modelling procedure for infiltrated felt involves calculation of the fourth rank compliance contributions tensors for fibers and pores. It consists of the following two steps. First, the effective compliance tensor of randomly distributed fibers in the pyrolytic carbon matrix is obtained in closed form. For this purpose, the non-interaction and Mori–Tanaka predictions of the overall material properties are used. The effective material parameters of the fiber/matrix mixture were calculated for different volume fractions of fibers. The results of these calculations show that for the fiber volume fractions below 20%, both predictions are very close. From the microscopic observations it is known that the volume fraction of fibers in the studied composites is 12% and thus any of the considered micromechanical schemes can be used.

Second, the pores approximated as spheroids are embedded in the homogenized material. To calculate the compliance tensor of a spheroidal pore, the Eshelby solution is used. For the purpose of numerical calculations, a random distribution of pores was simulated using a software generator of random numbers. Microscopic observations show that the total porosity in this kind of composites is not higher than 15% which justifies the non-interaction approach used in the simulations. The material parameters of the composite with different volume fractions of pores have been evaluated. Numerical simulations show that the assumption of prolate spheroids (assumption that only prolate pore shapes are present in the microstructure) produces higher prediction of the effective elastic modulus of the composite than the assumption of the oblate spheroids. Since both shapes are present in the actual microstructure, it is expected that the effective stiffness of the composite will be bounded by "prolate" and "oblate" estimates.

Acknowledgements

The present study was performed in the Center of Excellence 551 in Research on "Carbon from the gas phase: elementary reactions, structures and materials." Financial support by the German Research Foundation (DFG) is gratefully acknowledged. The second author (I.T.) also acknowledges the support of the US Fulbright Scholar Program during the final stages of this research.

References

[1] Papenburg U. Faserverstärkte keramische Werkstoffe. In: Kriegesmann J, editor. Technische Keramische Werkstoffe. Köln: Deutscher Wirtschaftsdienst; 1994 [Chapter 4.4.1.0].

[2] Guellali M, Oberacker R, Hoffmann MJ. Influence of the matrix microstructure on the mechanical properties of CVI-infiltrated carbon fiber felts. Carbon 2005;43(9):1954–60 .
[3] Guellali M. Einfluss der Abscheide- und Heißpressbedingungen auf die Mikrostruktur und Eigenschaften von CVI-CFC-Werkstoffen. PhD Thesis, Schriftenreihe des Instituts für Keramik im Maschinenbau, IKM 040, Universität Karlsruhe (TH); 2003.
[4] Benzinger W, Hüttinger KJ. Chemistry and kinetics of chemical vapor infiltration of pyrocarbon-V: infiltration of carbon fiber felt. Carbon 1999;37(6):941–6.
[5] Tsukrov I, Piat R, Novak J, Schnack E. Micromechanical modeling of porous carbon/carbon composites densified by chemical vapor infiltration. Mech Adv Mater Struct 2005;12(1):1537–6532.
[6] Nemat-Nasser S, Hori M. Micromechanics: overall properties of heterogeneous materials. Elsevier; 1999.
[7] Eroshkin O, Tsukrov I. On micromechanical modeling of particulate composites with inclusions of various shapes. Int J Solids Struct 2005;42(2):409–27.
[8] Mori M, Tanaka K. Average stress in matrix and average elastic energy of materials with misfitting inclusions. Acta Metall 1973;21(5):571–4.
[9] Benveniste Y. A new approach to the application of Mori–Tanaka's theory in composite materials. Mech Mater 1987;6(2):147–57.
[10] Mura T. Micromechanics of defects in solids. Kluwer Academic Publishers; 1998.
[11] Kachanov M, Shafiro B, Tsukrov I. Handbook of elasticity solutions. Kluwer Academic Publishers; 2004.
[12] Kostka H, Birkle S, Küsebauch W. Pyrokohlenstoff-Eigenschaften und Anwendung. Mat-wiss U Werkstofftech 1989;20:92–100.
[13] Papadakis EP, Bernstein H. Elastic moduli of pyrolytic graphite. J Acoust Soc Am 1963;35(4):521–4.